Additive Manufacturing 22 (2018) 592–600

Contents lists available at ScienceDirect

Additive Manufacturing

journal homepage: www.elsevier.com/locate/addma

Full length article

The influence of aging temperature and aging time on the mechanical and tribological properties of selective laser melted maraging 18Ni-300 steel

Shuo Yin[a,*], Chaoyue Chen[b], Xingchen Yan[b,c], Xiaohua Feng[d], Richard Jenkins[a], Peter O'Reilly[a], Min Liu[c], Hua Li[d], Rocco Lupoi[a,*]

[a] Trinity College Dublin, the University of Dublin, Department of Mechanical and Manufacturing Engineering, Parsons Building, Dublin 2, Ireland
[b] ICB UMR 6303, CNRS, Universitie de Bourgogne Franche-Comté, UTBM, Belfort, 90010, France
[c] National Engineering Laboratory for Modern Materials Surface Engineering Technology, The Key Lab of Guangdong for Modern Surface Engineering Technology, Guangdong Institute of New Materials, Guangzhou 510651, PR China
[d] Ningbo Institute of Materials Technology and Engineering, Chinese Academy of Sciences, Ningbo 315201, PR China

ARTICLE INFO

Keywords:
Selective laser melting (SLM)
Additive manufacturing (AM)
XRD
Microstructure
Ultimate tensile strength (UTS)
Wear rate

ABSTRACT

Selective laser melting (SLM) is an additive manufacturing and 3D printing technology which offers flexibility in geometric design and rapid production of complex structures. Maraging steels have high strength and good ductility, and therefore have been widely used in aerospace and tooling sectors for many years. This work aims to study the influence of aging temperature and aging time on the microstructure, mechanical property (hardness, strength and ductility) and tribological property of SLM maraging 18Ni-300 steel. The results reveal that the aging conditions had a significant impact on the strength and wear-resistance of the SLM maraging steel. The optimal aging conditions for the SLM maraging steel produced in this work were 490 °C for 3 h under which strength and wear-resistance were maximised. Lower or higher aging temperature led to under-aging or over-aging phenomena, reducing the strength and wear-resistance performance. Shorter or longer aging time also resulted in the decrease of strength and wear-resistance performance of the SLM maraging steel as compared with the optimal conditions. The variation of the mechanical and tribological properties is primarily due to changes in phase compositions and microstructures of the SLM maraging steels.

1. Introduction

Selective laser melting (SLM) is an additive manufacturing and 3D printing technology, which is predominantly used for the production of metal-based components (i.e., pure metals, alloys and metal matrix composites). With SLM, a high-power laser beam is used to selectively melt powder feedstock according to a pre-defined computer-aided design (CAD) model. The liquid melt pool created by the laser rapidly cools to form a solid track which when combined with neighbouring tracks and layers, can form near-net-shape components [1]. SLM offers several unique advantages over other conventional manufacturing processes, such as flexibility in geometric design, rapid production of components with complex geometry and high spatial resolution (e.g., turbine disc and cellular lightweight structures), customization of products at an acceptable cost (due to the lack of tooling), and little material waste through the recycling of unprocessed powder [1–3]. Components fabricated via SLM under optimized manufacturing parameters can be almost fully dense and have equivalent mechanical properties as compared with wrought counterparts. SLM is hence well recognized as a novel manufacturing technology of the future.

Steels have excellent mechanical properties such as high strength, toughness and good machinability, and have been widely used in the modern industry. Due to their excellent wettability and low reflectivity, steels are candidate alloys of high interest for SLM [1,2]. To date, a number of studies have been carried out to study the microstructure and properties of SLM steels, such as austenitic stainless steels [4–19], precipitation hardenable stainless steels [20–23] and maraging steels [24–35]. Among these, high-strength and high-ductility maraging steels have been widely used in aerospace and tooling sectors which has resulted in these alloys being a focus of SLM studies in recent years. Studies demonstrated that high-density and high-performance maraging steels can be produced through SLM using optimized laser parameters and scanning strategies [29,34–36]. SLM maraging steels typically have very fine cellular structure in the as-fabricated state due to the very high cooling rates and rapid solidification during manufacture [37–39]. Therefore, SLM maraging steels generally have higher yield strength, tensile strength and hardness as compared with wrought counterparts [28,29]. However, such high strength and low ductility

* Corresponding authors.
E-mail addresses: yins@tcd.ie (S. Yin), lupoir@tcd.ie (R. Lupoi).

https://doi.org/10.1016/j.addma.2018.06.005
Received 2 May 2018; Received in revised form 28 May 2018; Accepted 10 June 2018
Available online 15 June 2018

also results in a low transition fatigue life of the SLM maraging steel [40].

Aging treatment is known to be an effective way to improve the hardness and strength of precipitation hardenable alloys due to the formation of intermetallic precipitates [41,42]. In terms of SLM maraging steels, studies have confirmed that the microstructure and mechanical properties of SLM maraging steels can be improved through proper aging treatment [20,22,24–30,33]. The aged SLM maraging steels can have much higher strength than the as-fabricated steels with reduced ductility. Although existing studies have demonstrated the importance of aging treatment in improving the mechanical performance of SLM maraging steels, systematic investigations on the aging parameters (aging temperature and aging time) for SLM maraging steels are not prevalent. In addition, maraging steels are mainly used in aerospace, tooling and mold industries where the working environments are normally aggressive and excellent wear-resistance performance is necessary. Hence, investigations on the tribological properties of SLM maraging steels are also greatly needed. Considering the aforementioned points, this paper aims to explore the influence of aging temperature and aging time on the microstructure, mechanical properties (hardness, strength and ductility) and tribological property of SLM maraging steels.

2. Experimental methodology

2.1. Manufacturing procedure

Spherical maraging 18Ni-300 steel powder (EOS GmbH, Germany) with a size range of between 33 and 40 μm was used as the feedstock. Fig. 1a shows the surface morphology of the maraging steel powders observed by scanning electron microscope (SEM, Carl Zeiss ULTRA, Germany). Fig. 1b shows the cross-section of a maraging steel powder after etching. It can be seen in Fig. 1b that the microstructure of the maraging steel powder is dendritic which is a typical microstructure of rapidly cooled steels. EOS M290 SLM system (EOS GmbH, Germany) was used to produce the maraging steel samples. Experiments were performed in a nitrogen environment with substrate preheating to a temperature of 40 °C. Optimized scanning parameters were used in this experiments with a laser power of 285 W, a hatch distance of 110 μm, a laser beam speed of 960 mm/s, a laser spot diameter of 100 μm, and a layer thickness of 40 μm [29]. The laser scanning trajectory follows a zigzag pattern with an angle of 67° between adjacent layers. Fig. 2 shows a photograph of three SLM maraging 18Ni-300 steel samples manufactured using the optimized parameters, highlighting the reliability of these parameters. Note that these samples were only produced for demonstration purposes rather than mechanical or tribological testing. Following the manufacture of the maraging steel samples, aging treatment was carried out under various temperatures (from 390 to 590 °C) and time (from 1 to 7 h) without pre-solution treatment. The aging parameters were chosen based on the findings of previous studies [24,26,36]. Aging treatment and sample cooling were both performed in air.

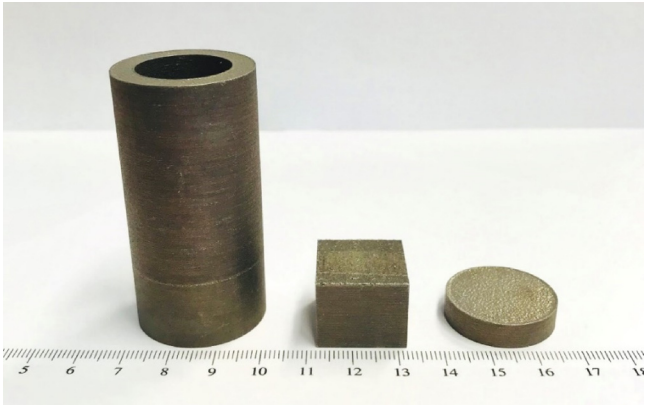

Fig. 2. Photo of three SLM maraging 18Ni-300 steel products manufactured using the optimized parameters.

2.2. Materials characterization

The relative density of the SLM maraging steel samples was measured by an analytical balance (ABZ 200C, PCE instruments, Germany) based on Archimedes principle using the following formula:

$$\frac{\rho_{SLM}}{\rho_{standard}} = \frac{\rho_{water} \bullet m_{SLM(air)}}{\rho_{standard} \bullet (m_{SLM(air)} - m_{SLM(water)})} \quad (1)$$

where, ρ_{SLM} is the density of SLM sample; $\rho_{standard}$ is the standard density of maraging steel; $m_{SLM(air)}$ is the weight of SLM sample in air; $m_{SLM(water)}$ is the weight of SLM sample in water; ρ_{water} is the density of water. Three samples were tested and averaged to determine the relative density. The cross-sectional microstructure of the SLM samples was studied using an optical microscope (OM) and SEM. As a preparation for the microstructure analysis, the samples were polished using standard metallographic procedures with the final polishing applied using 0.06 μm silica solution. Polished samples were etched with a modified Fry's reagent of 1 g $CuCl_2$, 25 ml HNO_3, 50 ml HCL and 150 ml water to observe and study the grain structure. To examine the phase transformation after aging treatment, the SLM samples were examined by an X-Ray diffractometer (XRD, Siemens D500, Germany) with the Co (λ = 1.789 Å) source at a current of 40 mA, voltage of 35kV, scanning step of 0.02° and scanning speed of 6 s per step. In order to accurately analyse the phase fraction of SLM maraging steels before and after aging, Rietveld analysis was conducted using JADE 6.0 software based on the measured XRD spectrum through phase retrieval, pattern fitting and Rietveld refinement.

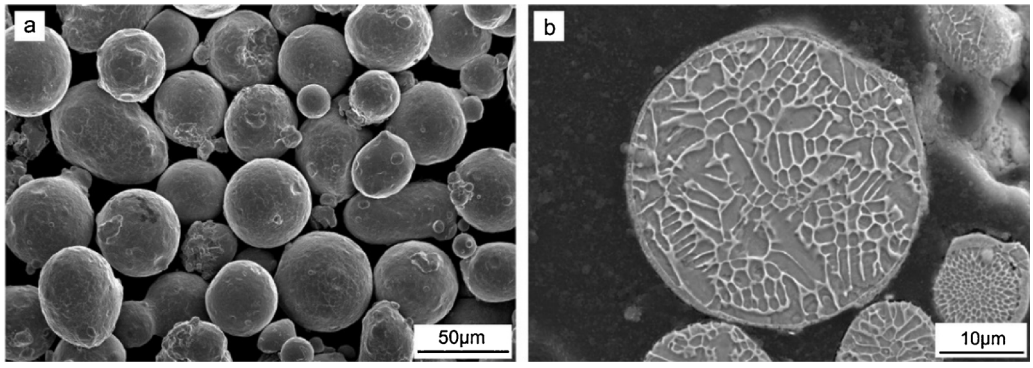

Fig. 1. Maraging 18Ni-300 steel powders used in the experiments. (a) surface morphology, and (b) cross-sectional view after etching.

2.3. Mechanical property test

The microhardness of the SLM maraging steel samples before and after aging treatment was tested using a Vickers hardness indenter (Mitutoyo, Japan) with a load of 500 g and dwell time of 10 s. Ten locations were tested on each sample, and the average value was considered as the microhardness. The tensile strength of the SLM maraging steel samples was measured by a universal tensile strength system (Instron 8801, UK) at a displacement rate of 10 mm/min as per ASTM E8 specification. The tensile specimens were produced in a dog-bone shape by SLM directly with a gauge length of 25 mm, gauge width of 5 mm and thickness of 2.2 mm. Ultimate tensile strength (UTS) and break elongation (EL) before and after aging treatment were determined based on the average value of three tensile samples for each aging parameter. The surface morphologies of the fractured tensile samples were then studied by SEM.

2.4. Tribological property test

The tribological property of the SLM maraging steel samples was measured using POD-2 pin-on-disc tribometer (CSEM Instruments, Switzerland) at room temperature. For accurate measurement of the wear rates, the sample surfaces were polished using silicon carbide first, followed by 6 µm diamond solution prior to the test, and the samples were then mounted on a carrier disc. A tungsten carbide ball with a diameter of 5 mm was used as a counterpart under a constant load of 5 N. The disk rotated at a linear speed of 10 mm/s. The material volume loss was calculated according to ASTM G 99 standard [43]. The wear rate was then calculated as the volume loss per unit load per traverse distance. The sliding distance and track diameter were set as 200 m and 5 mm, respectively. Three cross-sections were selected along the wear track and used to calculate the average wear rate.

3. Results and discussion

3.1. Microstructure of the as-fabricated SLM maraging steel

Fig. 3 shows the OM imaging of the etched cross-section of the as-fabricated SLM maraging steel in the horizontal (vertical to building direction, BD) and vertical planes (parallel to BD). During SLM, the cooling rate is inhomogeneous within a molten pool; the maximum cooling rate is located at the boundary of the molten pool where solidification is much faster than inner zones. This results in the occurrence of segregation, making the molten pool boundaries visible after etching [36]. From Fig. 3a, laser tracks with a width of approximately 80 µm and inter-track angle of 64° can be seen on the horizontal cross-section. In addition, semi-elliptical structures with a height of approximately 45 µm can be observed on the vertical cross-section from Fig. 3b, reflecting the shape of laser molten pool. The characteristics visible on the etched cross-sections are in agreement with the defined scanning parameters.

Fig. 4 shows SEM images of the cross-section of the as-fabricated SLM maraging steel (before and after etching) and the XRD spectrum. As can be seen in Fig. 4a, the SLM maraging steel exhibited very dense structure with few micro-defects. Defects are typically caused by unmelted powders and entrapment of gases in the molten pools during solidification [7,28]. The density measurement showed that the relative density of the SLM maraging steel was 99.22 ± 0.32%, which is quite close to the fully-dense bulk maraging steel. The etched cross-section in Fig. 4c and the high-magnification view in Fig. 4d reveals the grain structure of the as-fabricated SLM maraging steel. It is clearly shown that the microstructure of the as-fabricated SLM maraging steel is present in the form of very fine cellular structure with an intercellular spacing of hundreds of nanometres, which is in contrast to the larger microstructure of the feedstock powders (as shown in Fig. 1b). The formation of the fine microstructure is due to the extremely high cooling rate of the molten pool which prevents the formation of secondary dendrite arms during the solidification process [11]. The orientation of cellular structures was not uniform across all grains as shown in Fig. 4c where black dotted lines indicate the grain boundaries. Note that the cells are 3D in structure and they can be observed as either equiaxed or lath shaped in the 2D plane depending on the angle of view. Such fine cellular structure is a typical microstructure of SLM steels, which can lead to improvement of the hardness and strength of SLM steels as compared with conventionally manufactured steels [2]. In addition, from the XRD spectrum shown in Fig. 4b, a small fraction of retained austenite was detected in the as-fabricated SLM maraging steel. The retained austenite arose from the microsegregation of solute elements (particularly Ni) at cellular boundaries during solidification. The enrichment of Ni stabilizes the retained austenite [30], and thereby allowing the detection of the austenite phase.

3.2. Microstructure of the aged SLM maraging steel

To investigate the microstructure of the aged SLM maraging steel, Fig. 5 shows the SEM imaging of the etched cross-section of the SLM samples under various aging parameters. The XRD spectrum (Fig. 6) and the corresponding Rietveld Refinement analysis (Table 1) of the as-fabricated and aged SLM samples were also provided to assist the analysis. As can be seen from Fig. 5a-c, the aging temperature significantly influenced the microstructure of the SLM maraging steel. The microstructure under the lowest aging temperature of 390 °C (Fig. 5a) exhibited a similar cellular structure to the as-fabricated component (Fig. 4c). Precipitations in this circumstance were known to be mainly µ-, S- and X- intermetallic phases [44,45]. The volume fraction of austenite slightly increased from 1.6% in the as-fabricated state to 1.9% due to the occurrence of austenite reversion during aging treatment. As the aging temperature increased to 490 °C, the boundary of the cells

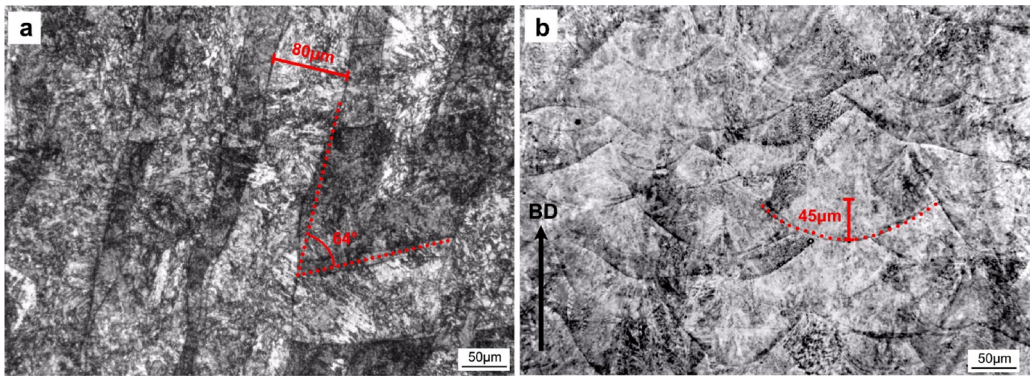

Fig. 3. Etched cross-section of the as-fabricated SLM maraging steel observed by OM. (a) horizontal view, and (b) vertical view.

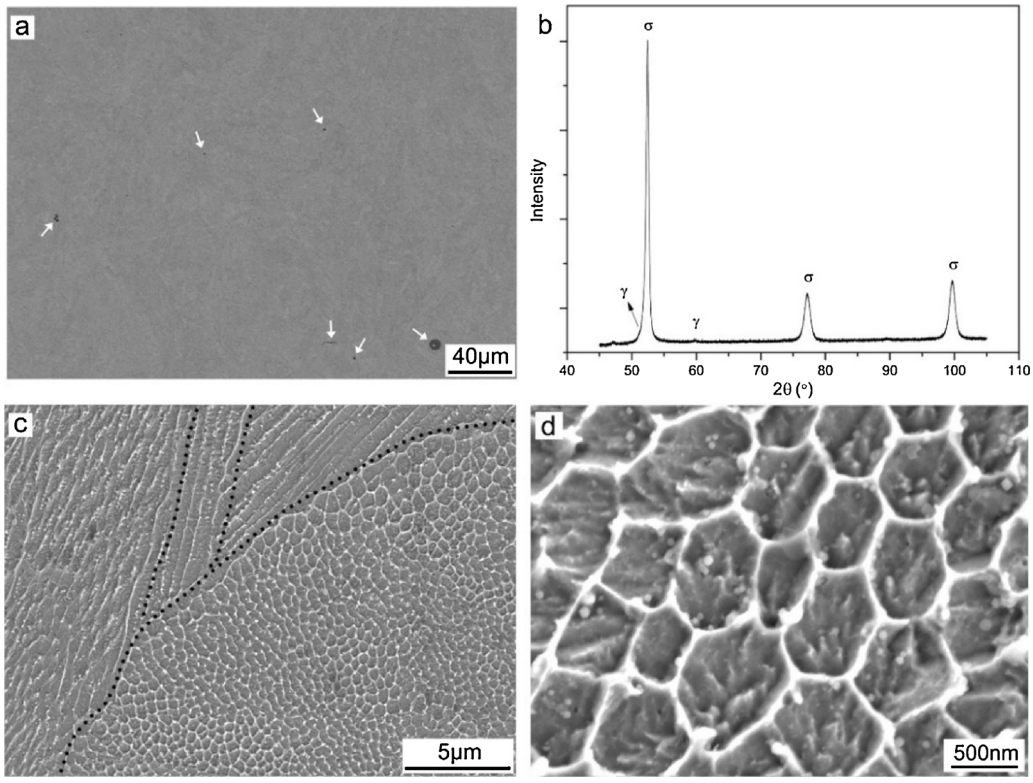

Fig. 4. Characterization of the as-fabricated SLM maraging steel. (a) cross-sectional SEM image before etching, (b) XRD spectrum, (c) cross-sectional SEM image after etching, and (d) high-magnification view of the cellular structure. Black dotted lines indicate grain boundaries.

became non-continuous as shown in Fig. 5b. Such changes were due to the precipitation of Ni-rich intermetallic phases (e.g., Ni_3Ti, Ni_3Mo, Ni_3Al), and the enhanced phase transformation of martensite to austenite (3.1%) at the cellular boundaries under high aging temperature [26,29,46]. The Ni_3Mo is formed initially upon aging due to its improved lattice fitting with the martensite. The Ni_3Ti is also rapidly formed during the aging due to the interaction between Ti and Ni. The Ni_3Al was formed through the substitution of the remaining Ti by Al [29]. Further increasing the aging temperature to 590 °C resulted in the obvious over-aging phenomenon. The microstructure exhibited very thick boundaries as shown in Fig. 5c due to the extremely prominent reversion of martensite to austenite [44]. The volume fraction of austenite phase increased to 65.8% when aged under 590 °C. In addition, the decomposition of Ni_3(Mo, Ti) phases and consequent precipitation of Fe_2Mo phase occurred at the same time, which also contributes to the austenite reversion [24,44].

As compared with increasing the aging temperature, increasing aging time posed a less significant impact on the microstructure. As can be seen from Fig. 5b and d–f, the microstructure of the SLM maraging steel under different aging times demonstrated a similar pattern, showing cellular structures with non-continuous cell boundaries. The cell boundaries became less defined with increasing the aging time.

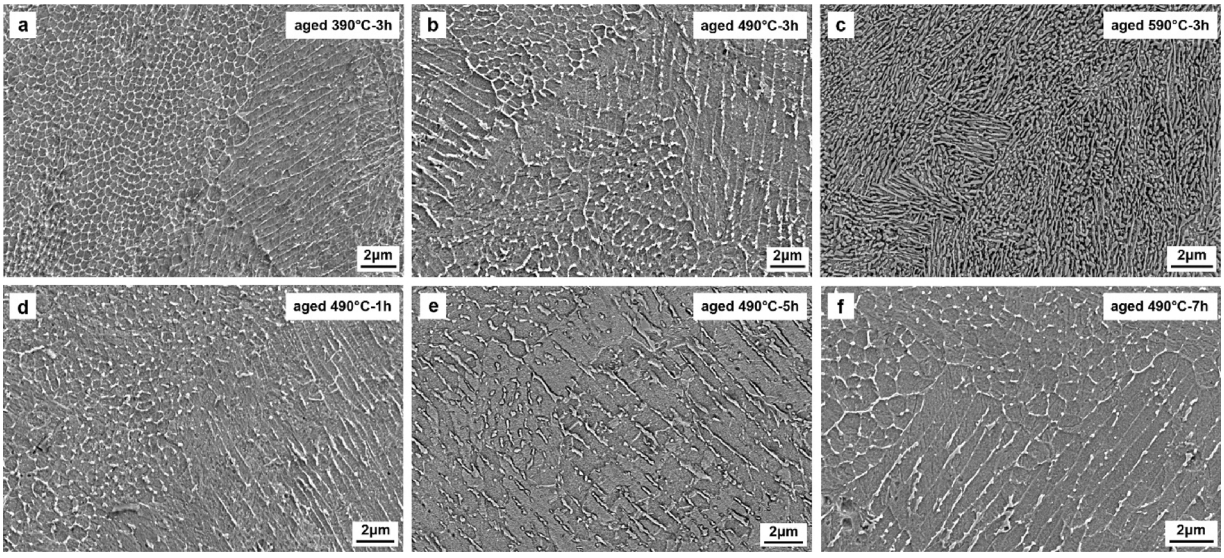

Fig. 5. SEM images of the etched cross-section of the aged SLM maraging steel under various aging temperatures and times. (a) 390 °C for 3 h, (b) 490 °C for 3 h, (c) 590 °C for 3 h, (d) 490 °C for 1 h, (e) 490 °C for 5 h, (f) 490 °C for 7 h.

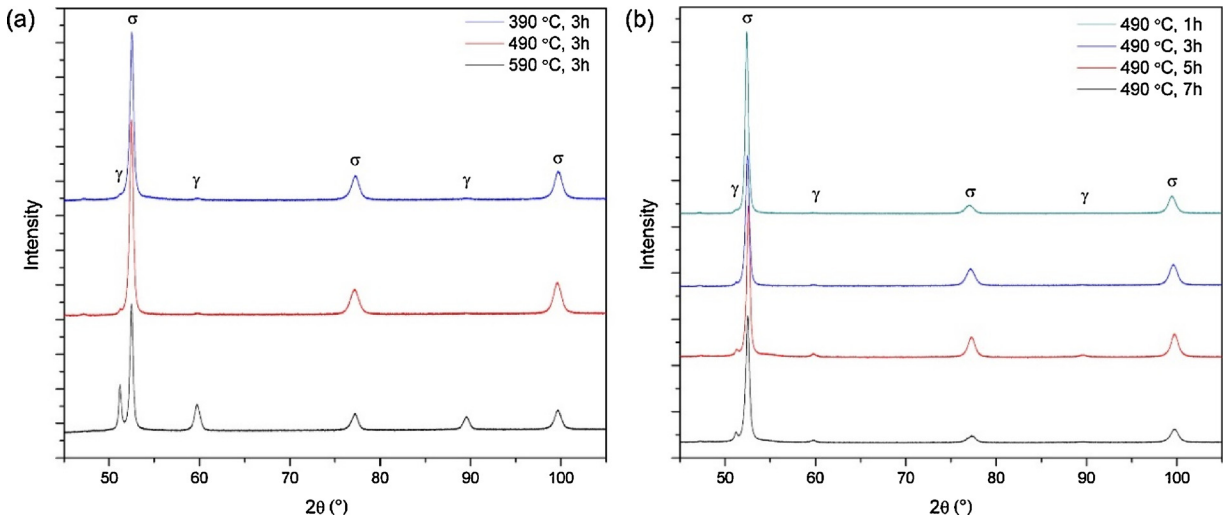

Fig. 6. XRD spectrum of the aged SLM maraging steel under (a) various aging temperatures and (b) various aging times.

Table 1
The volume of martensite (α) and austenite (γ) of the as-fabricated and aged SLM maraging steel under various aging conditions.

	α phase (%)	γ phase (%)	Error
As-fabricated	98.4	1.6	< 4.4%
Aged (390 °C, 3 h)	98.1	1.9	< 4.8%
Aged (490 °C, 3 h)	96.9	3.1	< 4.8%
Aged (590 °C, 3 h)	34.2	65.8	< 5.0%
Aged (490 °C, 1 h)	97.1	2.7	< 3.0%
Aged (490 °C, 5 h)	90.2	9.8	< 3.7%
Aged (490 °C, 7 h)	85.6	14.4	< 2.2%

This may be due to the enhanced reversion of martensite to austenite at longer aging time as listed in Table 1. However, significant over-aging did not occur. Even with the longest aging time of 7 h, the volume fraction of austenite was only 14.4%, much lower than in the case of 590 °C aging for 3 h. This fact clearly suggests that the microstructure and phase transformation of the SLM maraging steel is more sensitive to aging temperature than aging time.

3.3. Mechanical properties

Fig. 7a shows the effect of aging temperature on the hardness of the SLM maraging steel. It is clear that the hardness increased immediately after aging treatment due to the occurrence of precipitation hardening [24–26]. The peak hardness was achieved when the aging temperature was 490 °C due to the precipitation of Ni_3(Ti, Mo). Lower aging temperature (390 °C) resulted in under-aging featured by the precipitation of μ-, S- and X- intermetallic phases, while higher aging temperature (590 °C) led to over-aging featured by the decomposition of the Ni_3 (Ti, Mo) [44,45] and the formation of extensive revered austenite phase as listed in Table 1. Both phenomena can result in the reduction of hardness compared to the peak value. Fig. 7b shows the effect of aging time on the hardness of the SLM maraging steel. The hardness increased rapidly after aging for 1 h and marginally increased at an aging time of 3 h after which the hardness slightly reduced. This is because the shorter aging time resulted in less precipitations and therefore insufficient strengthening effect, while longer aging time led to more austenite phase and thus reduced strengthening effect. The variation of the hardness with the aging temperature and time is in agreement with the above microstructure and phase analysis.

Figs. 8 and 9 shows the effect of aging temperature and time on the stress-strain curves and tensile properties of the SLM maraging steel, respectively. As can be seen from Figs. 8a and 9a, under-aging at the temperature of 390 °C and over-aging at the temperature of 590 °C resulted in lower UTS. The UTS reduced after reaching the peak value at the aging time of 3 h as shown in Fig. 9b. The trend of the UTS first increasing to a peak and then decreasing with the aging temperature and time are similar to that of the hardness data in Fig. 7. It also can be seen in Figs. 8 and 9 that the increment in the UTS came with a reduction in the ductility. EL exhibited an inverse trend when compared

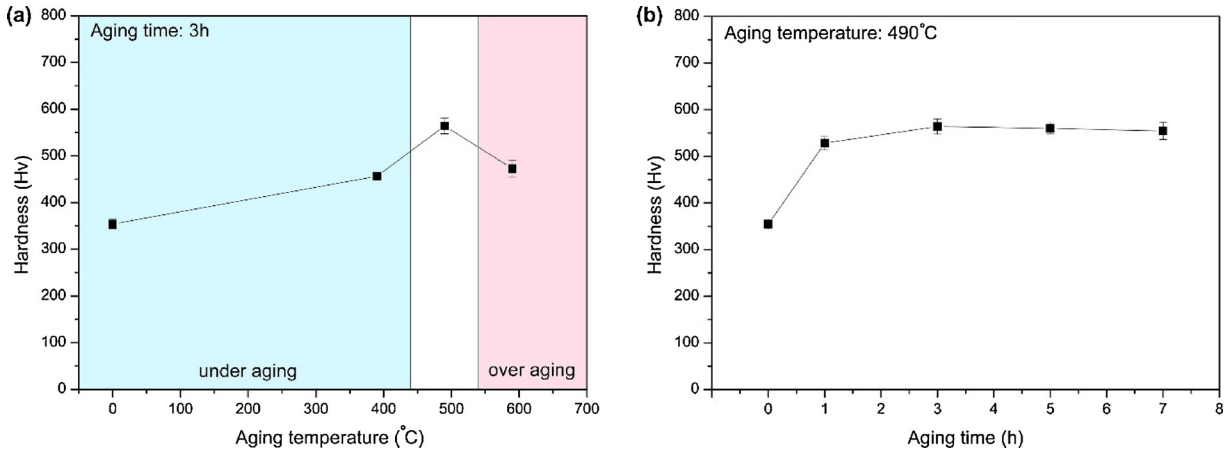

Fig. 7. Effect of (a) aging temperature and (b) aging time on the hardness of the SLM maraging steel.

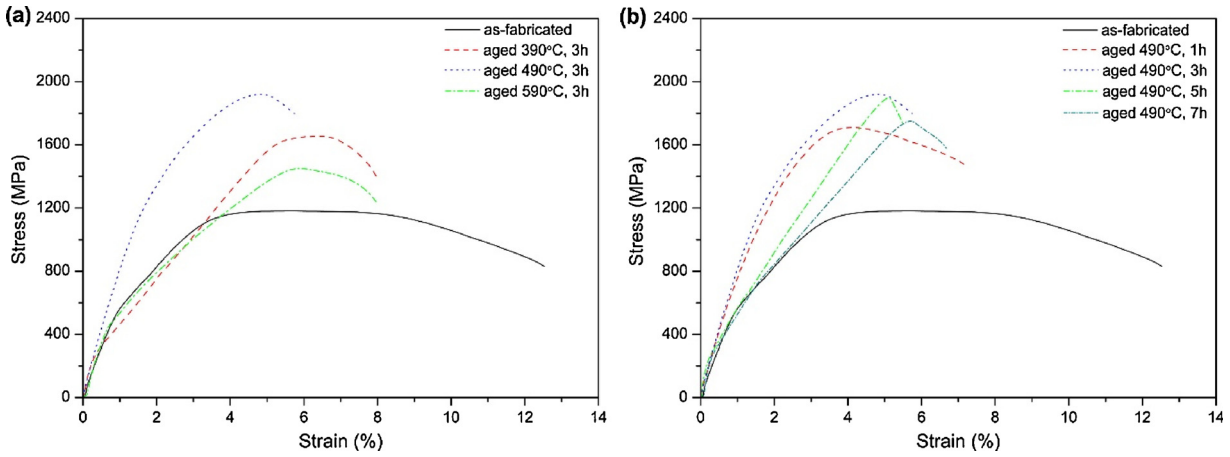

Fig. 8. Effect of (a) aging temperature and (b) aging time on the stress-strain curves of the SLM maraging steel.

to the UTS, reducing through with both aging time and aging temperature. A reduction in the EL with an increase in the UTS is typical of metals and cannot be prevented. Fig. 10 shows the comparison of the fractographic images of the tensile tested SLM maraging steel samples in the as-fabricated state and aged at 490 °C for 3 h (resulting in the highest UTS and lowest EL). The fracture surface of the as-fabricated sample reveals dimple-like features as shown in Fig. 10a, indicating ductile fracture mechanism. In the case of aged sample as shown in Fig. 10b, the fracture surface was characterized by both cleavage-like and dimple-like features, which suggests that the fracture mechanism was a combination of brittle and ductile fracture. This explains why the EL of the SLM maraging steel was reduced after aging. In addition, micro-sized balling defects formed during the SLM process can be seen on the fractured surface, which have been reported to have no significant effect on the properties of SLM components [47].

3.4. Tribological properties

In order to study the tribological properties of the SLM maraging steel before and after aging treatment, Fig. 11 shows the effect of aging temperature and time on the wear rate. The general variation trend of the wear rate with the aging parameters is inverse to that of the hardness and strength shown in Figs. 7 and 9. The wear rate of the SLM maraging steel reduced significantly after aging treatment due to the precipitation-strengthening, suggesting the improved wear-resistance performance. The best wear-resistance performance was achieved at the aging condition of 490 °C for 5 h. Lower aging temperature and shorter aging time resulted in higher wear rate due to reduced strengthening effect associated with these treatments. Note that aging at 490 °C for 3 h resulted in a slightly higher wear rate but would be a more economical aging treatment when considering the higher cost of a longer aging time. However, the small difference between these two tests may be caused by uncertainty during experimentation rather than differences between the effects of the aging process on the materials. In addition, aging at 490 °C for 3 h led to the highest hardness and tensile strength. Given these considerations, aging at 490 °C for 3 h is considered as the optimal aging parameters herein. It has to be noted that the proposed optimal aging parameter is not a strict optimal condition because it is obtained based on the limited testing parameters used in this work. However, this optimal parameter can be regarded as a reference for the future aging treatment of SLM maraging 18Ni-300 steel.

SEM images of the worn surface of the as-fabricated sample and aged sample (490 °C for 3 h) are provided in Fig. 12 to aid with the understanding of the wear mechanism of the SLM maraging steel before and after aging. For the as-fabricated sample, the worn surface was characterized by deep grooves and fragmented debris. EDX point analysis indicates that the fragmented debris was maraging steel. The worn features show that the as-fabricated sample experienced severe deformation and material peel-off during the sliding test, which indicates that abrasion was the primary wear mechanism [48]. Other features are evident for the aged sample indicating that a different wear mechanism is causing material removal. In contrast to the deep grooves, the worn surface is covered with an adhesion tribofilm. EDX point analysis confirms that the tribofilm was composed of both maraging steel and tungsten, which indicates that the pin ball was subject to severe wear during the sliding test due to the increased hardness of the aged SLM maraging steel. Such tribofilms can easily smear during the sliding test and protect the underlying surface from further wear [49]. Due to the

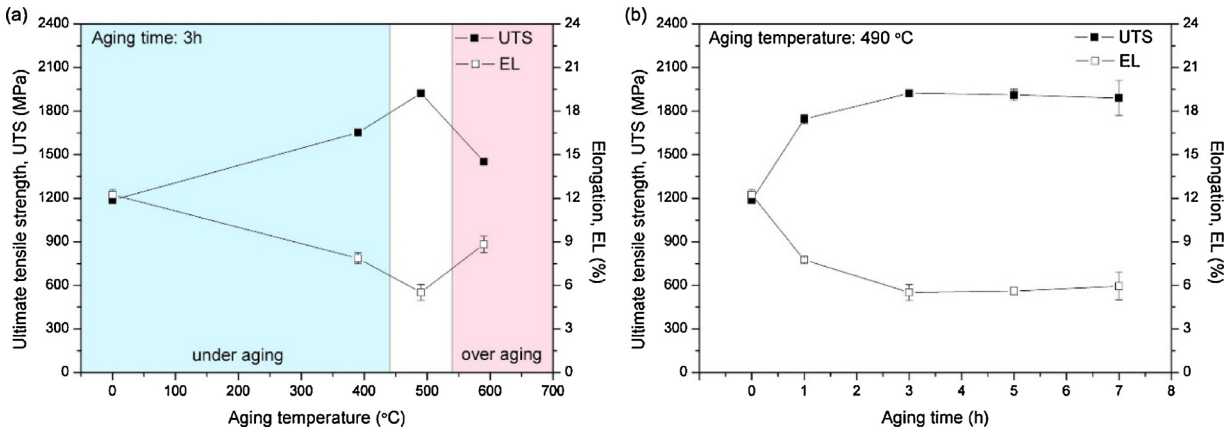

Fig. 9. Effect of (a) aging temperature and (b) aging time on the ultimate tensile strength and elongation of the SLM maraging steel.

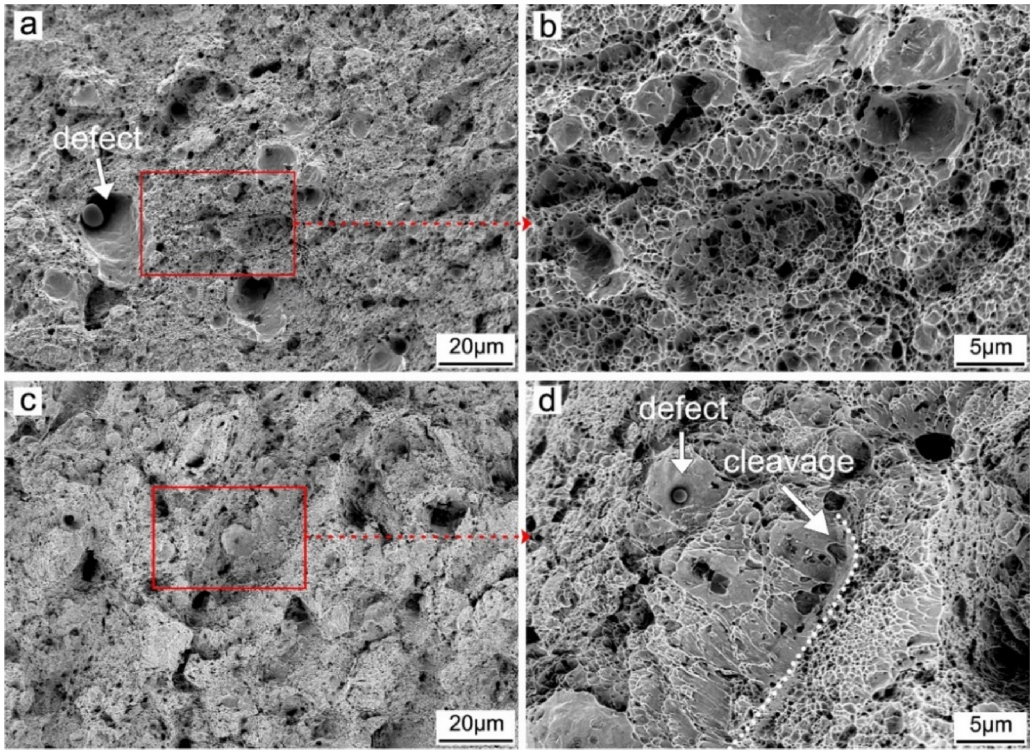

Fig. 10. Fractographic images of the SLM maraging steel tensile samples: (a, b) Fracture surface of as-fabricated maraging steel and magnified view, (c, d) Fracture surface of aged maraging steel and magnified view. White arrows indicate balling defects.

lubricating effect of the tribofilm, the coefficient of friction (COF) of the aged sample is always lower than that of the as-fabricated sample during the entire sliding test as shown in Fig. 13. As a consequence, the aged sample has a much lower COF (0.586 ± 0.071) than the as-fabricated sample (0.629 ± 0.061). Therefore, the wear mechanism of the aged sample is adhesion tribofilm.

4. Conclusions

Selective laser melting (SLM) is an additive manufacturing and 3D printing technology. In this work, experiments were carried out to study the influence of aging temperature and aging time on the microstructure, mechanical property (hardness, strength and ductility) and tribological property of SLM maraging 18Ni-300 steel. The main conclusions drawn from this work are listed below:

1 Dense maraging steel can be produced using SLM. The as-fabricated SLM maraging steel had a fine cellular microstructure with the intercellular spacing of hundreds of nanometres. A small fraction of austenite phase was found in the as-fabricated SLM maraging steel due to the microsegregation of solute elements during the solidification process.
2 Aging treatments have been shown to modify the phase composition and microstructure of the maraging steel produced with SLM. Increasing aging temperature and aging time resulted in more reversed austenite, different precipitations and thus different microstructures. In addition, the phase transformation and microstructure are more sensitive to aging temperature than aging time.
3 Aging treatment improved the strength of SLM maraging steel. There exists an optimal aging condition (490 °C for 3 h in this work) which can guarantee the highest strength of the SLM maraging steel. Lower or higher aging temperature led to under-aging or over-aging

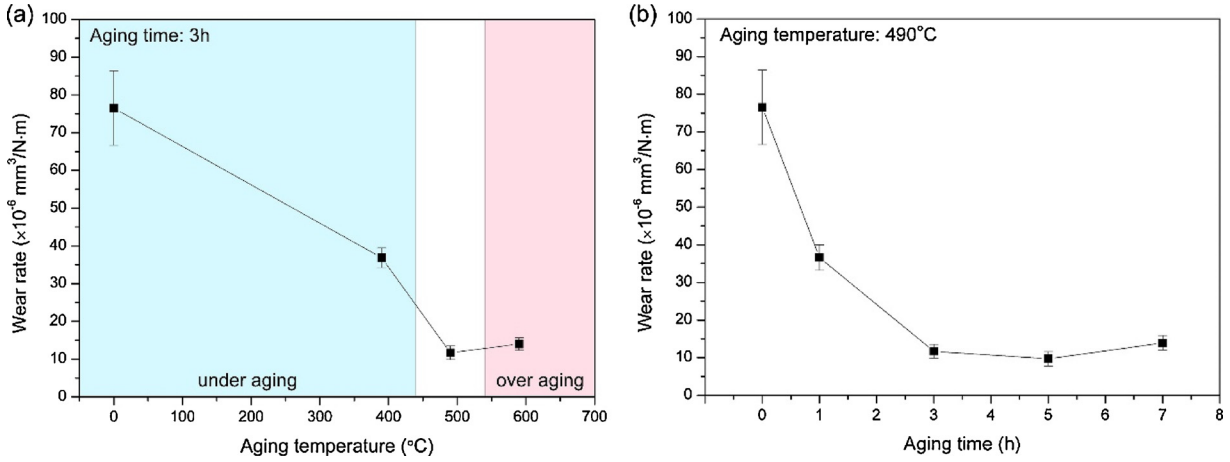

Fig. 11. Effect of (a) aging temperature and (b) time on the wear rate of the SLM maraging steel.

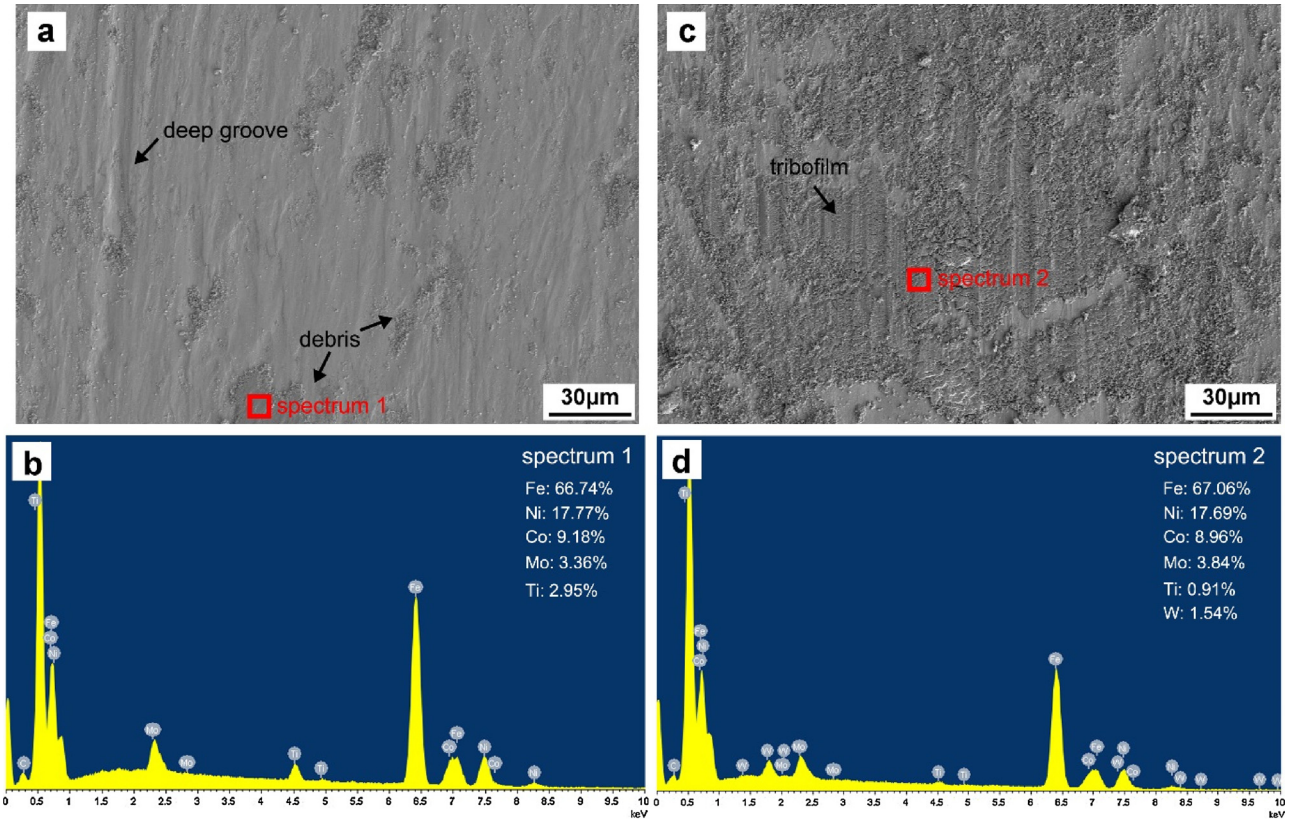

Fig. 12. Worn surfaces of the (a) as-fabricated and (b) aged SLM maraging steel (490 °C for 3 h) and (c, d) the corresponding EDX analysis. The atomic fraction of each element is also included in the figure.

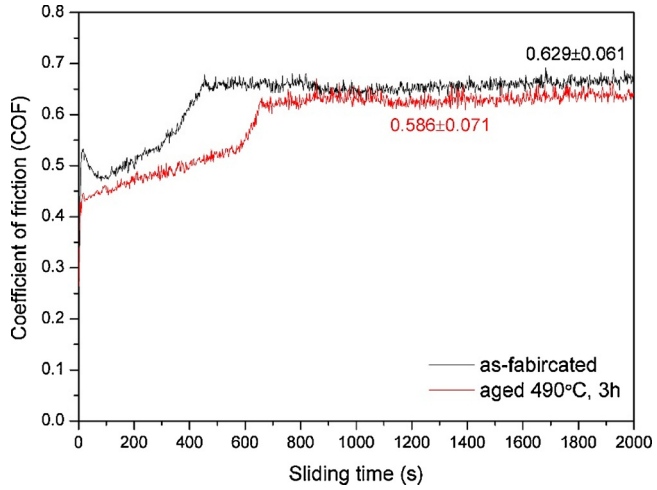

Fig. 13. Coefficient of friction of the as-fabricated and aged SLM maraging steels (490 °C for 3 h).

phenomena, reducing the strength of the SLM maraging steel. Shorter or longer aging time also resulted in the decrease of the strength of the SLM maraging steel as compared with the optimal aging time.

4 Aging treatment improved the tribological properties of the SLM maraging steel. Under the optimal aging conditions (490 °C for 3 h in this work), the SLM maraging steels had the best wear-resistance performance due to the improved hardness and strength. The wear mechanism of the SLM maraging steel changes from abrasion wear in the as-fabricated state to adhesion tribofilm in the optimally aged state.

Acknowledgments

The authors would like to thank the financial support from Irish Research Council project (GOIPD-2017-912), European Space Agency (4000112844/14/NL/FE), Sciences Platform Environment and Capacity Building Projects of GDAS (2016GDASPT-0206, 2017GDASCX-0202, 2017GDASCX-0111, 2018GDASCX-0402 and 2018GDASCX-0111); Guangzhou Project of Science & Technology (201604016109, 201704030111); Guangdong province Science and Technology Plan Projects (2015B010122004, 2015B090920003 2016B070701020, 2016B090916003, 2017A070702016, 2017B030314122 and 2017A070701027); Guangdong Natural Science Foundation (2016A030312015). Guangzhou Science and Technology Program (201510010095). We also thank the CRANN Advanced Microscopy Laboratory of Trinity College Dublin and Prof. Alain Billard from UTBM for the support in data analysis.

References

[1] T. Debroy, H.L. Wei, J.S. Zuback, T. Mukherjee, J.W. Elmer, J.O. Milewski, A.M. Beese, A. Wilson-heid, A. De, W. Zhang, Additive manufacturing of metallic components – process, structure and properties, Prog. Mater. Sci. 92 (2017) 112–224, http://dx.doi.org/10.1016/J.PMATSCI.2017.10.001.

[2] D. Herzog, V. Seyda, E. Wycisk, C. Emmelmann, Additive manufacturing of metals, Acta Mater. 117 (2016) 371–392, http://dx.doi.org/10.1016/j.actamat.2016.07.019.

[3] D.D. Gu, W. Meiners, K. Wissenbach, R. Poprawe, Laser additive manufacturing of metallic components: materials, processes and mechanisms, Int. Mater. Rev. 57 (2012) 133–164, http://dx.doi.org/10.1179/1743280411Y.0000000014.

[4] J. Suryawanshi, K.G. Prashanth, U. Ramamurty, Mechanical behavior of selective laser melted 316L stainless steel, Mater. Sci. Eng. A 696 (2017) 113–121, http://dx.doi.org/10.1016/j.msea.2017.04.058.

[5] Z. Sun, X. Tan, S.B. Tor, W.Y. Yeong, Selective laser melting of stainless steel 316L with low porosity and high build rates, Mater. Des. 126 (2017) 359, http://dx.doi.org/10.1016/j.matdes.2017.04.031.

[6] M. Ma, Z. Wang, X. Zeng, A comparison on metallurgical behaviors of 316L stainless steel by selective laser melting and laser cladding deposition, Mater. Sci. Eng. A 685

(2017) 265–273, http://dx.doi.org/10.1016/j.msea.2016.12.112.
[7] E. Liverani, S. Toschi, L. Ceschini, A. Fortunato, Effect of selective laser melting (SLM) process parameters on microstructure and mechanical properties of 316L austenitic stainless steel, J. Mater. Process. Technol. 249 (2017) 255–263, http://dx.doi.org/10.1016/j.jmatprotec.2017.05.042.
[8] H. Alsalla, L. Hao, C. Smith, Fracture toughness and tensile strength of 316L stainless steel cellular lattice structures manufactured using the selective laser melting technique, Mater. Sci. Eng. A 669 (2016) 1–6, http://dx.doi.org/10.1016/j.msea.2016.05.075.
[9] Y. Zhong, L. Liu, S. Wikman, D. Cui, Z. Shen, Intragranular cellular segregation network structure strengthening 316L stainless steel prepared by selective laser melting, J. Nucl. Mater. 470 (2016) 170–178, http://dx.doi.org/10.1016/j.jnucmat.2015.12.034.
[10] A. R??ttger, K. Geenen, M. Windmann, F. Binner, W. Theisen, Comparison of microstructure and mechanical properties of 316 L austenitic steel processed by selective laser melting with hot-isostatic pressed and cast material, Mater. Sci. Eng. A 678 (2016) 365–376, http://dx.doi.org/10.1016/j.msea.2016.10.012.
[11] D. Wang, C. Song, Y. Yang, Y. Bai, Investigation of crystal growth mechanism during selective laser melting and mechanical property characterization of 316L stainless steel parts, Mater. Des. 100 (2016) 291–299, http://dx.doi.org/10.1016/j.matdes.2016.03.111.
[12] A. Ahmadi, R. Mirzaeifar, N.S. Moghaddam, A.S. Turabi, H.E. Karaca, M. Elahinia, Effect of manufacturing parameters on mechanical properties of 316L stainless steel parts fabricated by selective laser melting: a computational framework, Mater. Des. 112 (2016) 328–338, http://dx.doi.org/10.1016/j.matdes.2016.09.043.
[13] K. Saeidi, X. Gao, F. Lofaj, L. Kvetková, Z.J. Shen, Transformation of austenite to duplex austenite-ferrite assembly in annealed stainless steel 316L consolidated by laser melting, J. Alloys Compd. 633 (2015) 463–469, http://dx.doi.org/10.1016/j.jallcom.2015.01.249.
[14] C. Yan, L. Hao, A. Hussein, P. Young, D. Raymont, Advanced lightweight 316L stainless steel cellular lattice structures fabricated via selective laser melting, Mater. Des. 55 (2014) 533–541, http://dx.doi.org/10.1016/j.matdes.2013.10.027.
[15] K. Guan, Z. Wang, M. Gao, X. Li, X. Zeng, Effects of processing parameters on tensile properties of selective laser melted 304 stainless steel, Mater. Des. 50 (2013) 581–586, http://dx.doi.org/10.1016/j.matdes.2013.03.056.
[16] B. Zhang, L. Dembinski, C. Coddet, The study of the laser parameters and environment variables effect on mechanical properties of high compact parts elaborated by selective laser melting 316L powder, Mater. Sci. Eng. A 584 (2013) 21–31, http://dx.doi.org/10.1016/j.msea.2013.06.055.
[17] R. Li, Y. Shi, Z. Wang, L. Wang, J. Liu, W. Jiang, Densification behavior of gas and water atomized 316L stainless steel powder during selective laser melting, Appl. Surf. Sci. 256 (2010) 4350–4356, http://dx.doi.org/10.1016/j.apsusc.2010.02.030.
[18] M.L. Montero Sistiaga, S. Nardone, C. Hautfenne, J. Van Humbeeck, Effect of heat treatment of 316L stainless steel produced by selective laser melting (SLM), 27th Annu. Int. Solid Free. Fabr. Symp. - An. Addit. Manuf. Conf. Solid Free. Fabr. Symp. (2016), pp. 558–565.
[19] Y.M. Wang, T. Voisin, J.T. McKeown, J. Ye, N.P. Calta, Z. Li, Z. Zeng, Y. Zhang, W. Chen, T.T. Roehling, R.T. Ott, M.K. Santala, P.J. Depond, M.J. Matthews, A.V. Hamza, T. Zhu, Additively manufactured hierarchical stainless steels with high strength and ductility, Nat. Mater. (2017), http://dx.doi.org/10.1038/nmat5021 nmat5021..
[20] Z. Hu, H. Zhu, H. Zhang, X. Zeng, Experimental investigation on selective laser melting of 17-4PH stainless steel, Opt. Laser Technol. 87 (2017) 17–25, http://dx.doi.org/10.1016/j.optlastec.2016.07.012.
[21] M. Akita, Y. Uematsu, T. Kakiuchi, M. Nakajima, R. Kawaguchi, Defect-dominated fatigue behavior in type 630 stainless steel fabricated by selective laser melting, Mater. Sci. Eng. A 666 (2016) 19–26, http://dx.doi.org/10.1016/j.msea.2016.04.042.
[22] T. LeBrun, T. Nakamoto, K. Horikawa, H. Kobayashi, Effect of retained austenite on subsequent thermal processing and resultant mechanical properties of selective laser melted 17-4 PH stainless steel, Mater. Des. 81 (2015) 44–53, http://dx.doi.org/10.1016/j.matdes.2015.05.026.
[23] L.E. Murr, E. Martinez, J. Hernandez, S. Collins, K.N. Amato, S.M. Gaytan, P.W. Shindo, Microstructures and properties of 17-4 PH stainless steel fabricated by selective laser melting, J. Mater. Res. Technol. 1 (2012) 167–177, http://dx.doi.org/10.1016/S2238-7854(12)70029-7.
[24] K. Kempen, E. Yasa, L. Thijs, J.P. Kruth, J. Van Humbeeck, Microstructure and mechanical properties of selective laser melted 18Ni-300 steel, Phys. Procedia 12 (2011) 255–263, http://dx.doi.org/10.1016/j.phpro.2011.03.033.
[25] E.A. Jägle, P.-P. Choi, J. Van Humbeeck, D. Raabe, Precipitation and austenite reversion behavior of a maraging steel produced by selective laser melting, J. Mater. Res. 29 (2014) 2072–2079, http://dx.doi.org/10.1557/jmr.2014.204.
[26] R. Casati, J. Lemke, A. Tuissi, M. Vedani, Aging behaviour and mechanical performance of 18-Ni 300 steel processed by selective laser melting, Metals (Basel) 6 (2016) 218, http://dx.doi.org/10.3390/met6090218.
[27] Y. Bai, Y. Yang, D. Wang, M. Zhang, Influence mechanism of parameters process and mechanical properties evolution mechanism of maraging steel 300 by selective laser melting, Mater. Sci. Eng. A 703 (2017) 116–123, http://dx.doi.org/10.1016/j.msea.2017.06.033.
[28] J. Suryawanshi, K.G. Prashanth, U. Ramamurty, Tensile, fracture, and fatigue crack growth properties of a 3D printed maraging steel through selective laser melting, J. Alloys Compd. 725 (2017) 355–364, http://dx.doi.org/10.1016/j.jallcom.2017.07.177.
[29] C. Tan, K. Zhou, W. Ma, P. Zhang, M. Liu, T. Kuang, Microstructural evolution, nanoprecipitation behavior and mechanical properties of selective laser melted high-performance grade 300 maraging steel, Mater. Des. 134 (2017) 23–34, http://dx.doi.org/10.1016/j.matdes.2017.08.026.
[30] P. Kürnsteiner, M.B. Wilms, A. Weisheit, P. Barriobero-Vila, E.A. Jägle, D. Raabe, Massive nanoprecipitation in an Fe-19Ni-xAl maraging steel triggered by the intrinsic heat treatment during laser metal deposition, Acta Mater. 129 (2017) 52–60, http://dx.doi.org/10.1016/j.actamat.2017.02.069.
[31] M. Yakout, A. Cadamuro, M.A. Elbestawi, S.C. Veldhuis, The selection of process parameters in additive manufacturing for aerospace alloys, Int. J. Adv. Manuf. Technol. 92 (2017) 2081–2098, http://dx.doi.org/10.1007/s00170-017-0280-7.
[32] R. Branco, J. Costa, F. Berto, S. Razavi, J. Ferreira, C. Capela, L. Santos, F. Antunes, Low-cycle fatigue behaviour of AISI 18Ni300 maraging steel produced by selective laser melting, Metals (Basel) 8 (2018) 32, http://dx.doi.org/10.3390/met8010032.
[33] Y. Bai, Y. Yang, Z. Xiao, D. Wang, Selective laser melting of maraging steel : mechanical properties development and its application in mold, Rapid Prototyp. J. 24 (3) (2018) 623–629, http://dx.doi.org/10.1108/RPJ-05-2017-0104.
[34] A.G. Demir, P. Colombo, B. Previtali, From pulsed to continuous wave emission in SLM with contemporary fiber laser sources: effect of temporal and spatial pulse overlap in part quality, Int. J. Adv. Manuf. Technol. 91 (2017) 2701–2714, http://dx.doi.org/10.1007/s00170-016-9948-7.
[35] A.G. Demir, B. Previtali, Investigation of remelting and preheating in SLM of 18Ni300 maraging steel as corrective and preventive measures for porosity reduction, Int. J. Adv. Manuf. Technol. (2017) 1–13, http://dx.doi.org/10.1007/s00170-017-0697-z.
[36] J. Mutua, S. Nakata, T. Onda, Z.-C. Chen, Optimization of selective laser melting parameters and influence of post heat treatment on microstructure and mechanical properties of maraging steel, Mater. Des. 139 (2017) 486–497, http://dx.doi.org/10.1016/j.matdes.2017.11.042.
[37] S. Pauly, L. Löber, R. Petters, M. Stoica, S. Scudino, U. Kühn, J. Eckert, Processing metallic glasses by selective laser melting, Mater. Today 16 (2013) 37–41, http://dx.doi.org/10.1016/j.mattod.2013.01.018.
[38] H.Y. Jung, S.J. Choi, K.G. Prashanth, M. Stoica, S. Scudino, S. Yi, U. Kühn, D.H. Kim, K.B. Kim, J. Eckert, Fabrication of Fe-based bulk metallic glass by selective laser melting: a parameter study, Mater. Des. 86 (2015) 703–708, http://dx.doi.org/10.1016/j.matdes.2015.07.145.
[39] K.G. Prashanth, J. Eckert, Formation of metastable cellular microstructures in selective laser melted alloys, J. Alloys Compd. 707 (2017) 27–34, http://dx.doi.org/10.1016/j.jallcom.2016.12.209.
[40] R. Branco, J. Costa, F. Berto, S. Razavi, J. Ferreira, C. Capela, L. Santos, F. Antunes, Low-cycle fatigue behaviour of AISI 18Ni300 maraging steel produced by selective laser melting, Metals (Basel) 8 (2018) 32, http://dx.doi.org/10.3390/met8010032.
[41] P. Wang, H.C. Li, K.G. Prashanth, J. Eckert, S. Scudino, Selective laser melting of Al-Zn-Mg-Cu: heat treatment, microstructure and mechanical properties, J. Alloys Compd. 707 (2017) 287–290, http://dx.doi.org/10.1016/j.jallcom.2016.11.210.
[42] P. Wang, C. Gammer, F. Brenne, K.G. Prashanth, R.G. Mendes, M.H. Rümmeli, T. Gemming, J. Eckert, S. Scudino, Microstructure and mechanical properties of a heat-treatable Al-3.5Cu-1.5Mg-1Si alloy produced by selective laser melting, Mater. Sci. Eng. A 711 (2018) 562–570, http://dx.doi.org/10.1016/j.msea.2017.11.063.
[43] S. Dosta, M. Couto, J.M. Guilemany, Cold spray deposition of a WC-25Co cermet onto Al7075-T6 and carbon steel substrates, Acta Mater. 61 (2013) 643–652, http://dx.doi.org/10.1016/j.actamat.2012.10.011.
[44] J.M. Pardal, S.S.M. Tavares, V.F. Terra, M.R. Da Silva, D.R. Dos Santos, Modeling of precipitation hardening during the aging and overaging of 18Ni-Co-Mo-Ti maraging 300 steel, J. Alloys Compd. 393 (2005) 109–113, http://dx.doi.org/10.1016/j.jallcom.2004.09.049.
[45] R. Tewari, S. Mazumder, I.S. Batra, G.K. Dey, S. Banerjee, Precipitation in 18 wt% Ni maraging steel of grade 350, Acta Mater. 48 (2000) 1187–1200, http://dx.doi.org/10.1016/S1359-6454(99)00370-5.
[46] E.A. Jagle, Z. Sheng, P. Kurnsteiner, S. Ocylok, A. Weisheit, D. Raabe, Comparison of maraging steel micro- and nanostructure produced conventionally and by laser additive manufacturing, Materials (Basel). 10 (2017), http://dx.doi.org/10.3390/ma10010008.
[47] R. Li, J. Liu, Y. Shi, L. Wang, W. Jiang, Balling behavior of stainless steel and nickel powder during selective laser melting process, Int. J. Adv. Manuf. Technol. 59 (2012) 1025–1035, http://dx.doi.org/10.1007/s00170-011-3566-1.
[48] K.G. Prashanth, S. Kumar, S. Scudino, B.S. Murty, J. Eckert, Fabrication and response of Al70Y16Ni 10Co4 glass reinforced metal matrix composites, Mater. Manuf. Process. 26 (2011) 1242–1247, http://dx.doi.org/10.1080/10426914.2010.544824.
[49] D. Gu, Y.C. Hagedorn, W. Meiners, G. Meng, R.J.S. Batista, K. Wissenbach, R. Poprawe, Densification behavior, microstructure evolution, and wear performance of selective laser melting processed commercially pure titanium, Acta Mater. 60 (2012) 3849–3860, http://dx.doi.org/10.1016/j.actamat.2012.04.006.